Climate Change over the Extratropical Southern Hemisphere: The Tale from an Ensemble of Reanalysis Datasets

SILVINA A. SOLMAN

Centro de Investigaciones del Mar y la Atmósfera, Consejo Nacional de Investigaciones Científicas y Técnicas, and Departamento de Ciencias de la Atmósfera y los Océanos, Facultad de Ciencias Exactas y Naturales, Universidad de Buenos Aires, Buenos Aires, Argentina

ISIDORO ORLANSKI

Atmospheric and Oceanic Science Program, Princeton University, Princeton, New Jersey

(Manuscript received 21 August 2015, in final form 3 December 2015)

ABSTRACT

In this study, a set of five reanalysis datasets [ERA-Interim, NCEP–DOE AMIP-II reanalysis (R2), MERRA, the Twentieth Century Reanalysis (20CR), and the CFS Reanalysis (CFSR)] is used to provide a robust estimation of precipitation change in the middle-to-high latitudes of the Southern Hemisphere during the last three decades. Based on several metrics accounting for the eddy activity and moisture availability, an attempt is also made to identify the dynamical mechanisms triggering these changes during extended summer and winter seasons. To that aim, a weighted reanalysis ensemble is built using the inverse of the variance as weighting factors for each variable. Results showed that the weighted reanalysis ensemble reproduced the observed precipitation changes at high and middle latitudes during the two seasons, as depicted by the GPCP dataset. For the extended summer season, precipitation changes were dynamically consistent with changes in the eddy activity, attributed mostly to ozone depletion. For the extended winter season, the eddy activity and moisture availability both contributed to the precipitation changes, with the increased concentration of greenhouse gases being the main driver of the climate change signal.

In addition, output from a five-member ensemble of the high-resolution GFDL CM2.5 for the period 1979–2010 was used in order to explore the capability of the model in reproducing both the observed precipitation change and the underlying dynamical mechanisms. The model was able to capture the rainfall change signal. However, the increased availability of moisture from the lower levels controls the precipitation change during both summer and winter.

1. Introduction

Evidence of climate change in the Southern Hemisphere (SH) during the last 50 years has been discussed in several studies. The climate change signal has been identified from a variety of diagnostics, using near-surface temperatures, near-surface and upper-level winds, sea level pressure, storm tracks, and rainfall, among others (Bender et al. 2012; Fu et al. 2006; Fyfe et al. 2012; Solman and Orlanski 2014; Orlanski 2013; Gillett et al. 2013; among others). At the hemispheric scale, it has been recognized that climate change in the SH is associated with a poleward extension of the Hadley cell, a poleward shift of the westerlies and midlatitude storm tracks inducing drying and wetting conditions over the subtropical and subpolar regions, respectively (Fyfe et al. 2012; Gastineau et al. 2009). Recently, Solman and Orlanski (2014, hereafter SO14), based on results derived using the ERA-40 dataset, showed that precipitation changes from 1961 to 2000 over the subtropical and midlatitudes were partially explained by changes in the frontal activity, in response to the poleward shift of the storm tracks.

The increase of greenhouse gases (GHGs) and stratospheric ozone depletion have been recognized as the main drivers of the SH extratropical circulation changes (Polvani et al. 2011; Arblaster and Meehl 2006; Thompson and Solomon 2002; Arblaster et al. 2011). Orlanski (2013, hereafter O13) used both ERA-40 and global model simulations to demonstrate that the

Corresponding author address: Silvina A. Solman, CIMA (CONICET-UBA), Ciudad Universitaria, Pabellón II, 2do piso, C1428EGA, Buenos Aires, Argentina.
E-mail: solman@cima.fcen.uba.ar

DOI: 10.1175/JCLI-D-15-0588.1

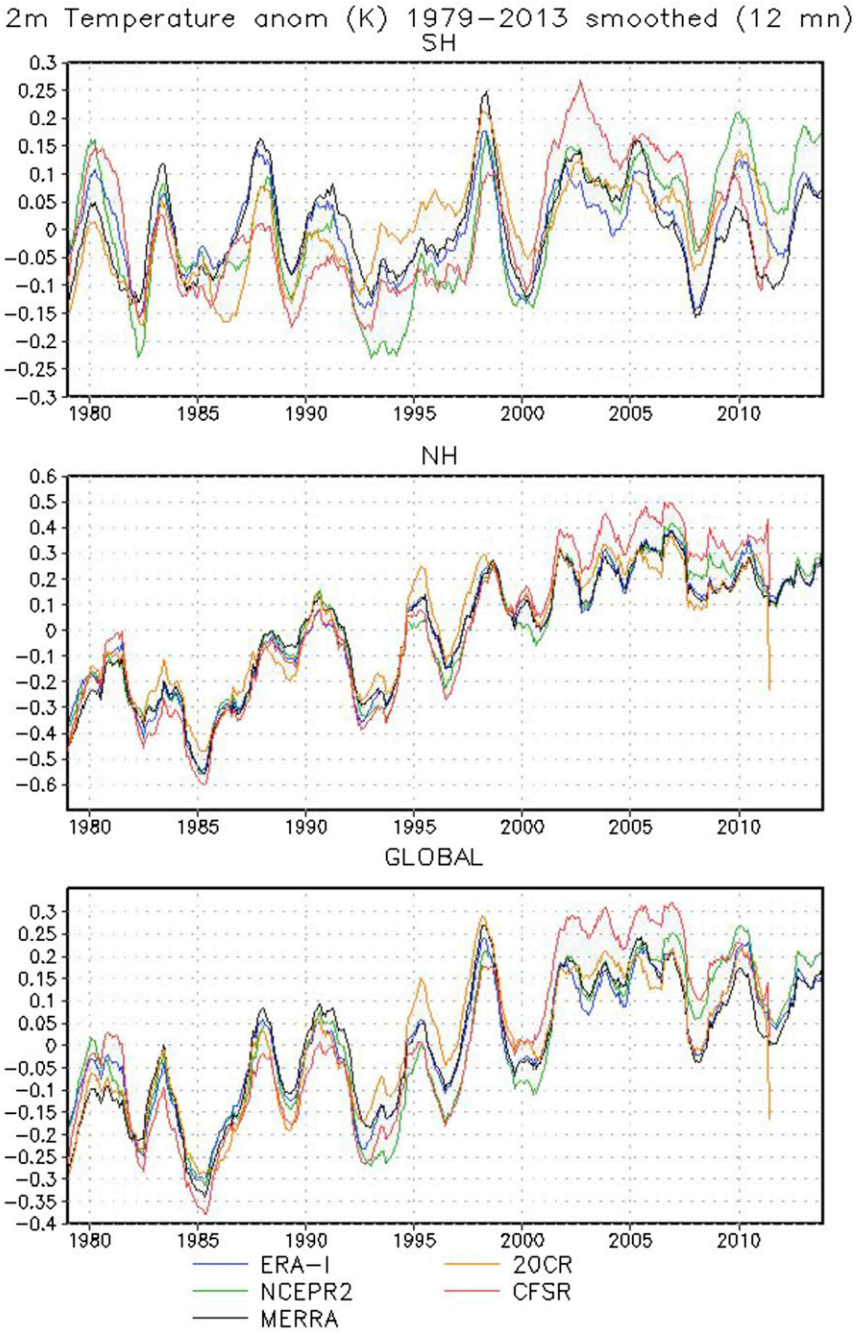

FIG. 1. Temporal evolution of the monthly mean 2-m temperature anomaly (K) for the period 1979–2013 averaged (top) over the Southern Hemisphere, (middle) over the Northern Hemisphere, and (bottom) globally for the five reanalysis datasets: ERA-I, MERRA, NCEPR2, 20CR, and CFSR. Anomalies were calculated with respect to the 1979–2013 monthly climatological mean, and time series were smoothed using a 12-month running mean.

positive trend in equatorial near-surface temperature associated with increasing GHGs (Bengtsson and Hodges 2011) and the negative trend in near-150-hPa temperature at high latitudes of the SH associated with stratospheric ozone depletion (Arblaster et al. 2011) both contributed to recent circulation changes in the SH. The stratospheric ozone depletion was the main driver of the increase in the low-level westerlies at high latitudes during summer, and both the increase of GHGs and ozone depletion triggered changes in the

asymmetric component of SH circulation in summer and winter. Gillett et al. (2013) also found that changes in GHGs, aerosols, and ozone have each made distinct significant contributions to observed SLP trends over the past 60 years over low latitudes as well as high latitudes.

The strongest limitation when dealing with the identification and attribution of long-term trends in the SH at the hemispheric scale is the lack of high-quality data. Recall that the SH is characterized by large oceanic areas, and surface-based observations are scarce, mainly over the extratropical latitudes. Although several reanalysis datasets are now available that span long periods (more than 50 yr), the quality of their products is still under debate, particularly for characterizing long-term trends in the SH, as discussed in Trenberth et al. (2011). Moreover, only since the 1980s has the availability of satellite information allowed for improved quality of the reanalysis products; however, large discrepancies among different reanalysis datasets still exist (Bosilovich et al. 2008; Chelliah et al. 2011; Lorenz and Kunstmann 2012; Paek and Huang 2012). It is accepted that changes over time in the observing system and in the type of data assimilated may lead to spurious changes in the reanalysis fields. For example, Fig. 1 displays the temporal evolution of the 2-m temperature from 1979 to 2013 averaged over the SH, over the Northern Hemisphere (NH), and globally, from several reanalysis datasets. The figure shows that every reanalysis display increasing temperatures for both SH and NH, in agreement with observations, although the consistency among reanalyses is better for the NH, including the well-known pause in the NH warming since the early 2000s (Trenberth and Fasullo 2013). Moreover, the SH has a considerable larger variability and also larger spread compared with the NH, together with a very small temperature trend. It is also important to keep in mind that observational products, such as precipitation estimates from merged satellite and rain gauge analysis, may also display discrepancies in the climate change signal. Accordingly, we need to recognize that we need to be creative in order to build a robust estimation of the climate change signal in the SH based on the newer reanalysis products available. The mean motivation of this study is to give an objective evaluation of recent changes in the middle and high latitudes of the SH using a set of reanalyses.

Since precipitation seems to be a poorly constrained variable between different reanalysis datasets, and in order to identify the physical mechanisms that may explain the precipitation change signal in the SH, we will complement the analysis with several metrics that are dynamically and thermodynamically connected with precipitation in an attempt to reinforce the confidence of precipitation changes. Actually, it is not clear if the poleward shift of rainfall patterns in the SH is a result of fronts shifting poleward; humidity increasing because of the increase in sea surface temperatures associated with increasing GHGs; or a combination of these two effects. Accordingly, one topic of this study is to identify the relevance of dynamical and thermodynamical forcings that may explain rainfall changes.

In this study, we propose to make more consistent use of the different reanalysis datasets by combining them into an ensemble in order to determine in a more robust way the climate change signal in the SH. We also complement our presentation with results from a coupled climate model in order to evaluate if the model is capable of reproducing both the climate change features in the SH and the proposed underlying mechanisms that may explain them.

The manuscript is organized as follows: Section 2 describes the datasets, metrics, and methodology. Section 3 describes the results from the ensemble of reanalyses and from the climate model. A summary and conclusions are presented in section 4.

2. Data and methodology

a. Metrics

At the extratropical latitudes of the SH, much of the rainfall is associated with forced convection triggered by frontal systems (Catto et al. 2012; SO14; among others). Consequently, an appropriate measure of the eddy activity may be used to quantify fronts and their relation with rainfall. Using this metric, SO14 showed that more than 50% of the precipitation change in the SH was a result of a poleward shift of frontal activity. In the following, we apply several metrics to understand if rainfall changes are associated with changes in the eddy activity or changes in the moisture availability.

The VOR index was calculated as the monthly average of the daily cyclonic relative vorticity ξ at 850 hPa computed at each grid point. As we are interested in cyclonic systems, which are mostly associated with frontal activity, the relative vorticity was set to zero for anticyclonic cases:

$$\mathrm{VOR} = \begin{cases} \xi = -\dfrac{f}{|f|}\left(\dfrac{\partial v}{\partial x} - \dfrac{\partial u}{\partial y}\right), & \text{if} \quad \xi > 0 \\ 0, & \text{if} \quad \xi < 0 \end{cases}, \qquad (1)$$

where f is the Coriolis parameter and u and v are the zonal and meridional winds, respectively. The VOR index quantifies the cyclonic vorticity defined as positive for both the SH and NH.

The moist frontal activity (VORSPHUM) was defined as the monthly mean relative cyclonic vorticity (the index described above) multiplied by the monthly mean specific humidity at 850 hPa:

$$\text{VORSPHUM} = [\text{VOR}] \times \text{SPHUM}, \qquad (2)$$

where [ ] denotes the monthly mean operator and SPHUM is the monthly mean specific humidity at 850 hPa.

Finally, following Chang et al. (2013), the eddy activity index (DV24h) was defined as the square of the 24-h difference of the meridional velocity as follows:

$$\text{DV24h} = \{v(t + 24\,\text{h}) - v(t)\}^2. \qquad (3)$$

Note that DV24h represents synoptic-scale eddies, and VOR quantifies cyclonic vorticity centers associated with frontal activity; consequently, the former captures larger-scale features compared with the latter.

These eddy activity metrics are highly correlated with rainfall events from the subtropics to high latitudes of the SH. SO14 showed the connection between VOR and rainfall for selected events. In appendix A, some selected individual events show the close connection between eddy activity metrics and rainfall (Fig. A1). Given the evidence that rainfall is strongly associated with the eddy activity and the moisture availability, any change in the latter should explain changes in the former. This is one of the hypotheses that are being explored in the next section.

b. Data

Different datasets have been used in this study to characterize changes in rainfall and eddy activity in the SH. Monthly precipitation data come from the Global Precipitation Climatology Project (GPCP), version 2 (Huffman et al. 2009), for the period 1979–2010, which is used extensively for studying rainfall changes at global coverage. GPCP data combine various satellite-estimated rainfall products and rain gauge stations on a 2.5° × 2.5° global grid. We also use the Climate Prediction Center (CPC) Merged Analysis of Precipitation (CMAP; Xie and Arkin 1997), including the CMAP-enhanced dataset, that incorporates blended NCEP–NCAR reanalysis (R1) precipitation values. It is important to keep in mind the caveats with CMAP precipitation over the oceans, particularly for trends, as discussed in Trenberth et al. (2007).

Five reanalysis datasets have been used in this study, listed in Table 1, together with their horizontal resolution. Both monthly and daily data from the reanalysis datasets have been used for the 1979–2010 period.

TABLE 1. Reanalysis datasets used. The horizontal resolution indicated in the right column is for pressure levels variables. For some reanalysis datasets, rainfall is available in a Gaussian grid of roughly the resolution of the pressure level data.

Reanalysis dataset	Reference	Horizontal resolution (lon × lat)
ERA-I	Dee et al. (2011)	0.75° × 0.75°
NCEPR2	Kanamitsu et al. (2002)	1.875° × 1.875°
MERRA	Rienecker et al. (2011)	0.66° × 0.5°
20CR	Compo et al. (2011)	2° × 2°
CFSR	Saha et al. (2010)	0.5° × 0.5°

The ERA-Interim dataset (ERA-I) is a last-generation product from the European Centre for Medium-Range Weather Forecasts (ECMWF). The data assimilation system is based on a four-dimensional variational data assimilation (4D-Var) with a 12-h window and high horizontal resolution.

The NCEP–DOE AMIP-II reanalysis (R2) dataset (NCEPR2) is based on its predecessor R1, but with some improvements, fixed errors, and updated parameterizations of the physical processes. Because of its low resolution, limited assimilation of satellite radiances, and no assimilation of rainfall data, it is considered a first-generation reanalysis.

MERRA is the latest-generation reanalysis from the NASA Goddard Institute for Space Studies, based on the state-of-the-art GEOS version 5 (GEOS-5) data assimilation system, which includes many observing systems in a climate framework. A special focus is on historical analyses of the hydrological cycle on a broad range of time scales.

The Twentieth Century Reanalysis (20CR) is a retrospective reanalysis for the entire twentieth century based on specified SSTs and sea ice distribution and assimilating only surface observations of synoptic pressure.

The CFS Reanalysis (CFSR) dataset is a new reanalysis of the atmosphere, ocean, sea ice, and land based on a high-resolution coupled global model from NCEP. Radiance measurements from historical satellites are assimilated for the period 1979–present. CFSR also uses time-varying CO_2 concentrations.

We also use the output from the Geophysical Fluid Dynamics Laboratory (GFDL) Climate Model, version 2.5 (CM2.5), which is a fully coupled global climate model with a high horizontal resolution of about 50 km for the atmosphere (Delworth et al. 2012). The GFDL CM2.5 simulation includes five ensemble members forced with observational estimates of GHGs, anthropogenic aerosols, ozone, land use changes, solar irradiance, and volcanic eruptions for 1861–2005 and follows the IPCC representative concentration pathway 8.5

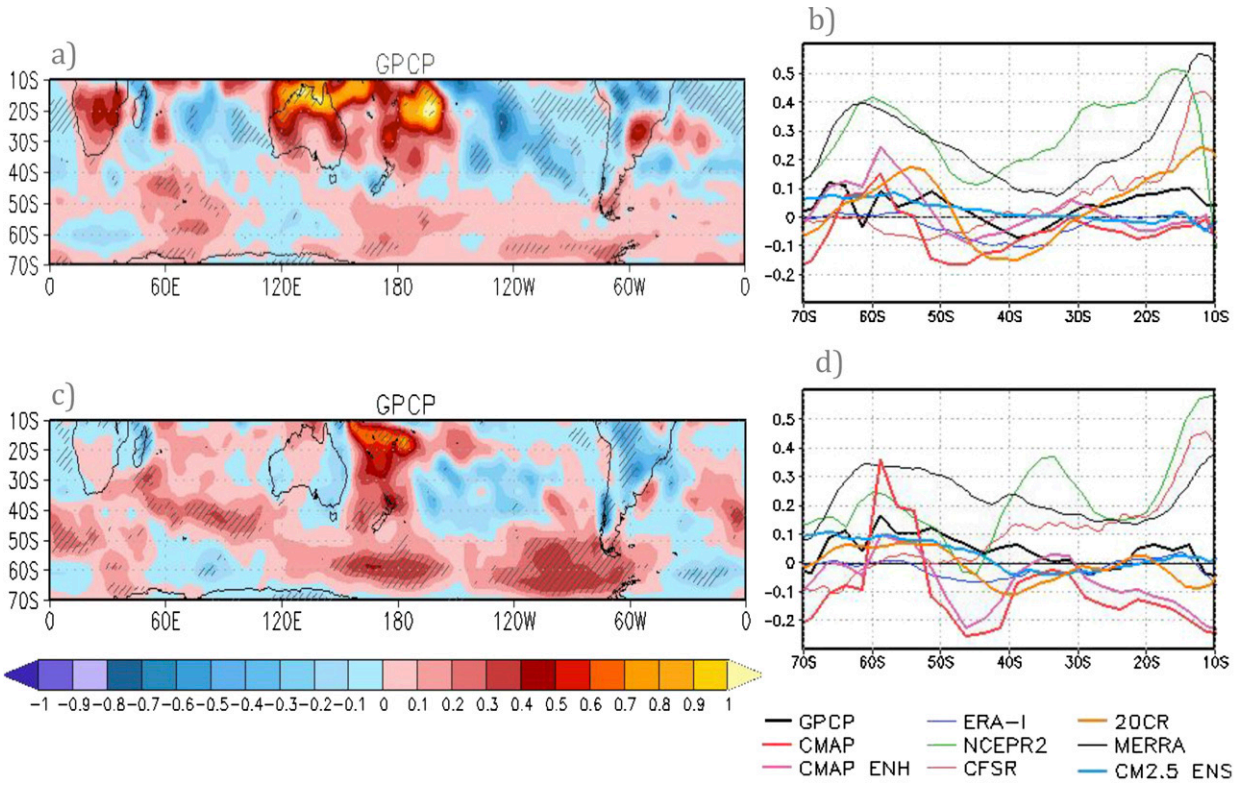

FIG. 2. Differences of the GPCP mean precipitation (mm day^{-1}) between the periods 1995–2010 and 1979–94 for the extended SH (a) summer and (c) winter seasons. Hatched areas indicate where the differences are statistically significant at the 95% level. (b),(d) Zonally averaged difference of precipitation (mm day^{-1}) as depicted by gridded precipitation datasets (GPCP, CMAP, and CMAP enhanced), reanalyses (ERA-I, NCEPR2, CFSR, 20CR, and MERRA), and the GFDL CM2.5 ensemble.

(RCP8.5) scenario from 2006 to 2100. Details of the simulations can be found in Delworth and Zeng (2014). In this study, we used monthly and daily outputs for the period from 1979 to 2010. Note that RCP8.5 concentrations are very similar to other RCPs over the period 2006–10.

The analysis is focused on two extended seasons: 1) October–March (ONDJFM), referred to as the warm season in the SH, and 2) April–September (AMJJAS), referred to as the cold season. The definition of the extended seasons is not only based on thermal considerations, but also takes into account the circulation regime and the eddy activity.

We start by examining the climate change signal depicted by each individual reanalysis dataset and compare it with the available observations. Figures 2b and 2d show the zonally averaged difference in the mean precipitation between the periods 1994–2010 and 1979–95 for extratropical latitudes of the SH during the two extended seasons. Note that GPCP displays the well-known midlatitude drying and high-latitude wetting pattern mainly during the warm season, in agreement with Fyfe et al. (2012) and SO14. Although there is a consensus on the overall precipitation change signal, mainly during the warm season, the discrepancies between different reanalyses and also between different satellite-based datasets are large. Because of the caveats on the CMAP precipitation products, we will use the GPCP dataset as reference (Trenberth et al. 2007). Note also that the reanalyses display large discrepancies between each other, including the sign of the precipitation difference. It is clear from Fig. 2 that an individual reanalysis should be used with caution when trying to identify consistent long-term trends of rainfall in the SH. To highlight the discrepancies between datasets, a Taylor diagram for precipitation over the latitudinal band from 40° to 15°S was computed based on the temporal behavior of the time series for the period from 1979 to 2010 (not shown) to identify the consistency in terms of the temporal correlation and variability with respect to the reference dataset (GPCP). It was found that, although CMAP and CMAP-enhanced datasets have a similar variability compared to the reference dataset, the correlation coefficients were close to 0.8. For the reanalysis datasets, the correlation coefficients lay between 0.4 and 0.6, and the variability was found to be 0.4–1.2 times the variability of the reference dataset (GPCP).

c. The ensemble of reanalyses

A simple variance-weighted average is used to build an ensemble of reanalyses, here called the reanalysis-weighted ensemble (REwens). For the weighted mean of a set of datasets for which each element X_i comes from a probability distribution with a given variance σ_i^2, one possible choice for the weights comes from

$$\overline{X} = \frac{\sum_{i=1}^{N} w_i X_i}{\sum_{i=1}^{N} w_i}, \tag{4}$$

where N is the number of datasets or reanalyses ($N = 5$) and $w_i = \sigma_i^{-2}$ is the weight of each individual reanalysis dataset for any given variable.

The variance of the ensemble mean is then

$$\sigma_{\overline{X}}^2 = \frac{1}{\sum_{i=1}^{N} w_i}. \tag{5}$$

Note that we are not assuming that the different reanalysis datasets are uncorrelated but that their differences probably are.

The reanalysis datasets used to compute REwens are listed in Table 1. Since the variance for each reanalysis depends on the variable to be considered, the weights to compute the ensemble will depend on the variable. More details on the rationale of using the weighted ensemble can be found in appendix B. The REwens was computed for the metrics described above: VOR, VORSPHUM, DV24h, and precipitation.

The ideal approach to create an ensemble of reanalysis datasets is to compare each reanalysis with observations and put more weight to those reanalyses that have similar variance compared with the observations. However, this is difficult to do in the SH because of the lack of observed data and because most of the metrics used in this study are not directly observed. Therefore, a compromise to the approach is to use a weight proportional to the inverse of the variance for each metric, assuming that the climatology of a metric will be better represented by a reanalysis with less variance. Since the variance-weighted average gives the best expected values of the climatological mean, it is expected that it also gives the best value for the mean differences. Finally, a weighted ensemble was also computed from the individual members of the GFDL CM2.5 simulations, based on the same considerations as for the REwens.

Note, however, that the REwens attempts to minimize the noise introduced by the diversity of assimilation methods and data in the reanalyses, but trying to highlight the real behavior of the atmosphere in terms of a climate change signal and natural variability. Conversely, the weighted ensemble based on multimember model simulations attempts to reduce the natural variability and highlight the forcing signal. Accordingly, even though the two ensembles are built following the same methodology, their results should be interpreted differently.

Although the 20CR may have some limitations, because it is based on assimilating surface observations only, the variables used in this study are evaluated at surface (precipitation) and at 850 hPa, which is very much influenced by near-surface circulation patterns. Moreover, inspection of the differences between the two periods considered (1979–94 and 1995–2010) in the set of variables analyzed for each individual reanalysis dataset shows an overall agreement, although changes depicted by 20CR are larger in magnitude compared with other reanalyses.

3. Results

a. The climate change signal in the SH as depicted by the REwens

Several studies devoted to characterizing the climate change signal in the SH have identified the poleward shift of the precipitation belt (usually referred to as the high-latitude moistening and subtropical drying pattern) as one of the most consistent features associated with the poleward shift in the westerlies and the poleward shift of the eddy activity (Fyfe et al. 2012; SO14; among others). Figures 2a and 2c display the difference between the mean precipitation for the period 1995–2010 and the period 1979–94, as depicted by the GPCP dataset, for both warm and cold seasons, respectively. Note that for the two seasons, rainfall increases poleward of about 45°S over the oceans and decreases from about 25° to 45°S. Rainfall increase over the high latitudes spreads over the southern Pacific Ocean and partially over the southern Atlantic and Indian Oceans, depending on the season. Note that the rainfall change pattern is more zonally symmetric during the warm season. The zonal-mean changes depicted in Fig. 2b,d capture this behavior.

As mentioned before, precipitation may change as a result of both dynamical and/or thermodynamical factors. Hence, the change in rainfall and several metrics representing both the dynamical and thermodynamical forcings as depicted by the REwens are displayed in Figs. 3 and 4 for the warm and cold seasons, respectively.

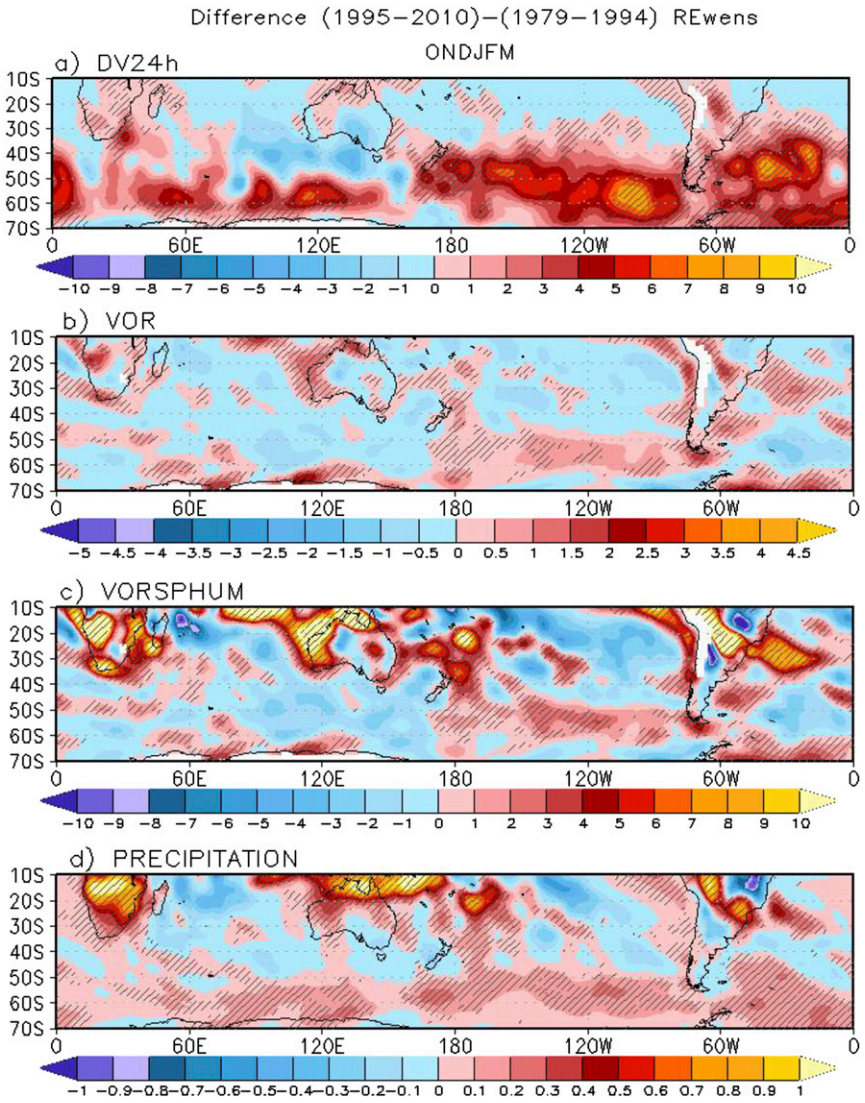

FIG. 3. Differences between 1995–2010 and 1979–94 during the extended summer season (ONDJFM) for (a) DV24h ($m^2 s^{-2}$); (b) VOR ($10^{-6} s^{-1}$); (c) VORSPHUM ($10^{-9} s^{-1}$); and (d) precipitation (mm day^{-1}) from the REwens. Hatched areas indicate where 4 out of 5 reanalyses depict positive differences.

Note that hatched areas in these figures indicate where at least four out of five reanalyses agree on positive differences. Two questions can be addressed: 1) To what extent is the REwens able to reproduce the observed precipitation changes? 2) What are the mechanisms that may explain them?

For the warm season (Fig. 3) the REwens shows a rainfall change pattern in agreement with GPCP observations (Fig. 2a). The pattern correlation coefficient between rainfall change from GPCP and REwens is 0.62, statistically significant at the 95% level. Note also that there is a general agreement between reanalyses on the sign of the precipitation change. Moreover, the rainfall increase over the high latitudes agrees with areas with increased eddy activity as characterized by both DV24h and VOR. Moreover, there is a consensus among different reanalyses on this behavior, although some reanalyses depict some inconsistencies between rainfall changes and eddy activity changes, as indicated by the lack of hatched areas. Recall that DV24h represents synoptic-scale eddies, and VOR captures cyclonic vorticity centers associated with frontal activity; hence, changes in DV24h are expected to be more spatially consistent than changes in VOR. Note also large areas over the southern Indian Ocean where VORSPHUM decreases and rainfall increases, suggesting that the

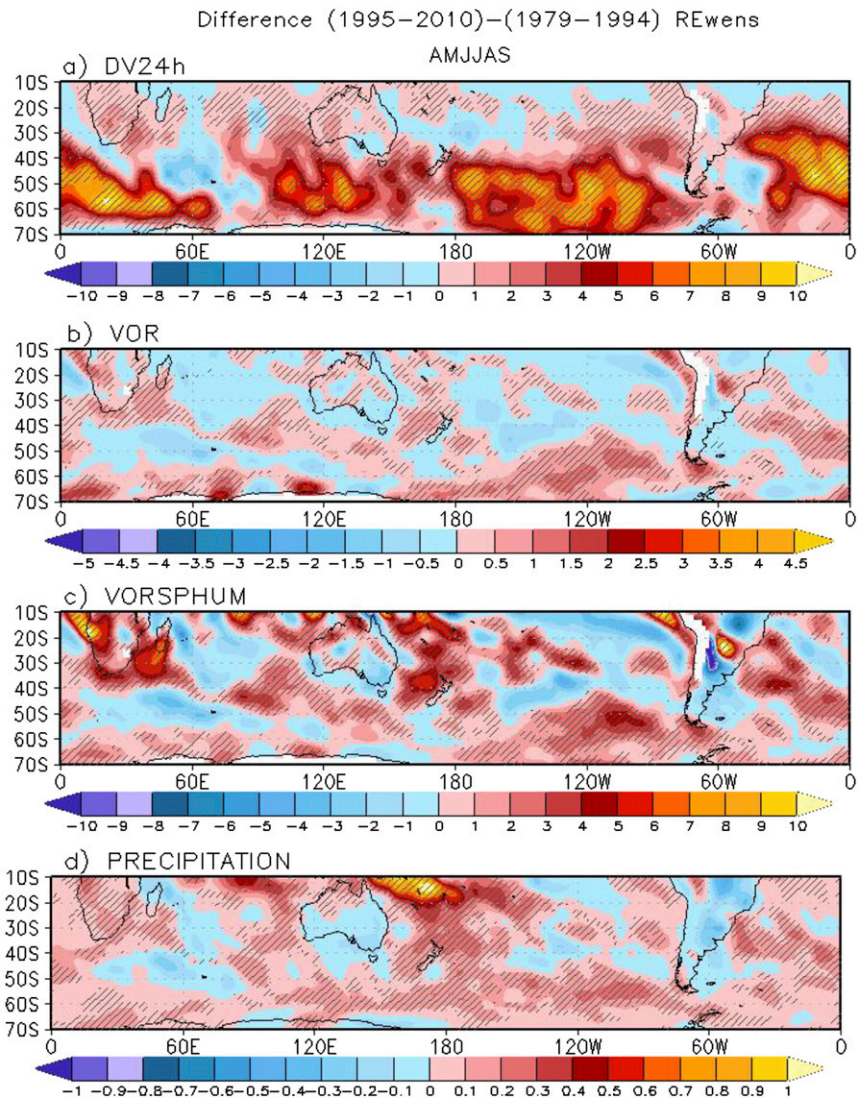

FIG. 4. As in Fig. 3, but for the extended winter season (AMJJAS).

rainfall increase is primarily associated with the increase in eddy activity and not with changes in humidity. Inspection of the role of changes in the specific humidity and VOR on changes in VORSPHUM reveals that the specific humidity decreases at high latitudes (from 50° to 70°S), and changes in VORSPHUM are dominated by changes in VOR. The rainfall decrease over the subtropics also agrees with areas where both DV24h and VOR are reduced. These changes in the eddy activity are closely related to changes in the tropospheric circulation, as discussed in SO14, and are consistent with the poleward shift of the storm tracks.

For the cold season (Fig. 4) the pattern of rainfall change for the REwens also agrees with the GPCP data displayed in Fig. 2 (with a pattern correlation coefficient of 0.46, statistically significant at the 95% level): the rainfall increase over the high latitudes is still apparent, but there are larger zonal asymmetries compared with the warm season. Over the midlatitudes, the REwens depicts drying regions over the central Pacific and the Indian Oceans and over southern South America and southeastern Australia, in agreement with both GPCP data and with results from regional studies (for Australia, Delworth and Zeng 2014; Cai et al. 2012). Note that there is a strong agreement between regions where rainfall increases (decreases) and the eddy activity and moisture availability increase (decrease). Changes in VOR and VORSPHUM agree with the spatial pattern of the precipitation change, suggesting that both the eddy activity and the availability of moisture contribute to the rainfall changes. The specific humidity increases

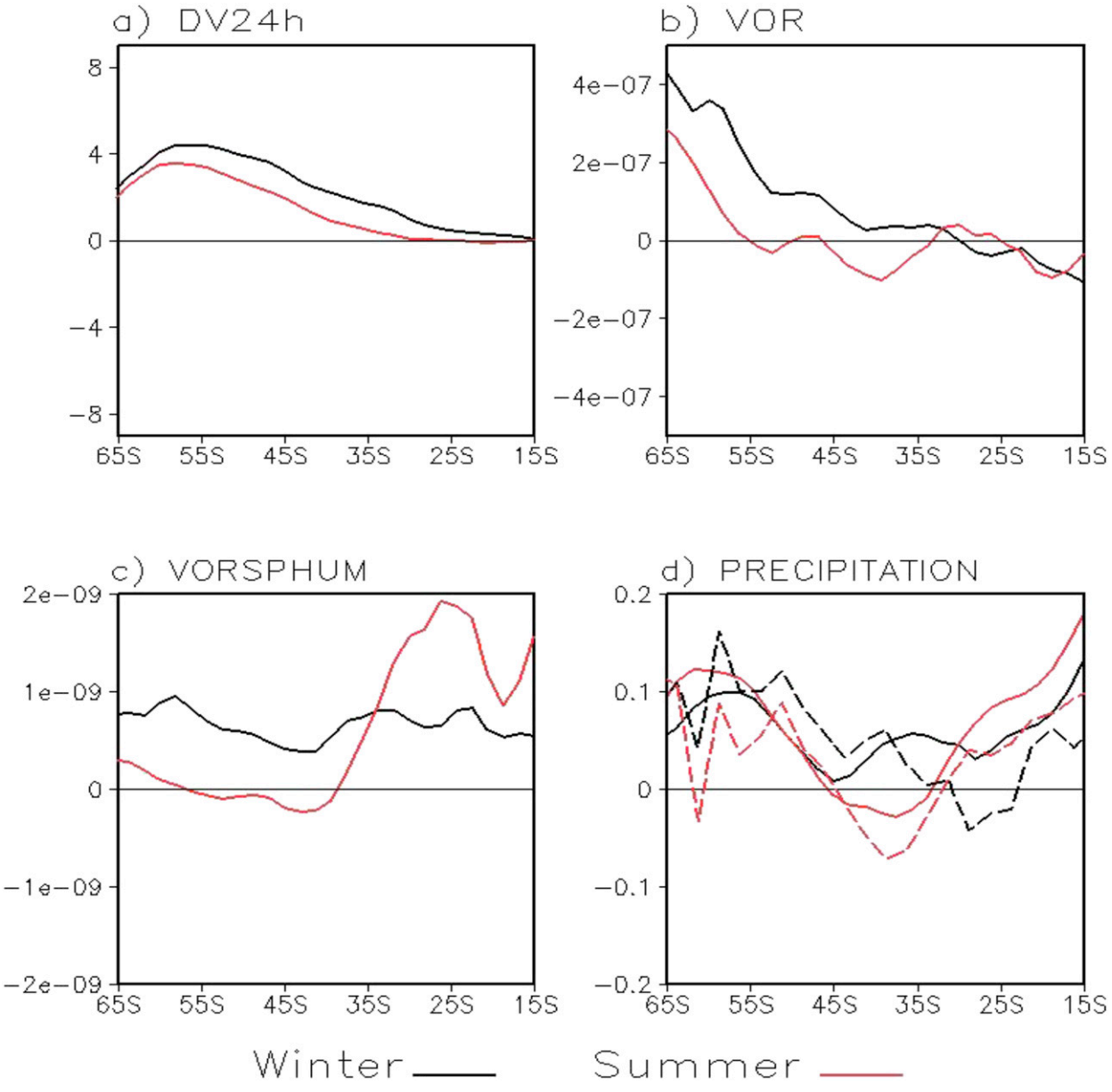

FIG. 5. Zonally averaged differences for summer (red) and winter (black) from REwens (solid lines) for (a) DV24h ($m^2 s^{-2}$); (b) VOR (s^{-1}); (c) VORSPHUM (s^{-1}); and (d) precipitation (mm day^{-1}). Dashed lines in (d) for GPCP data.

over much of the domain (not shown); however, as for the warm season, the changes in VORSPHUM are dominated by changes in VOR and, consequently, the increase in VORSPHUM is reinforced by the contribution of the specific humidity. Note also that there is a general agreement between reanalyses on this behavior, suggesting that the climate change signal is robust and physically consistent.

From Figs. 3 and 4 it is evident that some reanalysis datasets depict some discrepancies for the different metrics compared with the results described by the REwens and also some inconsistencies between the rainfall and the eddy activity changes. Theses inconsistencies suggest that an individual reanalysis provides a different picture of the changes both in rainfall and eddy activity in the SH, making it difficult to decide which reanalysis may be reliable for both characterizing the climate change signal in the SH and understanding the associated physical mechanisms.

The zonal-mean change of the set of metrics discussed above is shown in Fig. 5 for both the warm and cold seasons. Note the agreement between the zonal-mean

change in rainfall as depicted by the REwens and GPCP, particularly for summer. For the warm season, when the changes are more zonally symmetric, rainfall increase over the high latitudes is consistent with the increase of the eddy activity, as measured by DV24h and VOR. VORSPHUM shows no change at the high latitudes, suggesting that moisture content does not contribute to the rainfall change. For the cold season, Fig. 5 suggests that the rainfall increase at the high latitudes is not only associated with the increase of the eddy activity but also with the increase of the specific humidity at the low levels of the troposphere, probably associated with increased latent heat flux over the southern oceans, as identified by Yu et al. (2012).

To reinforce the relationship between eddy activity and rainfall, the temporal evolution of anomalies averaged over the midlatitudes of the Southern Hemisphere (from 60° to 30°S) during the two seasons was calculated for precipitation, DV24h, VOR, and VORSPHUM. The correlation coefficients between the time series of each metric of eddy activity and precipitation were found to be 0.54, 0.59, and 0.68 for ONDJFM, respectively, and 0.42, 0.56, and 0.61 for AMJJAS, respectively. All correlation coefficients are statistically significant at the 95% level. Similar results were found in SO14, who quantified the relationship between the interannual variability of the frontal activity, derived from the ERA-40 dataset, and precipitation over middle and high latitudes of the SH.

It was also found that the REwens reproduces the high-latitude upper-level cooling and the poleward shift of the zonal-mean circulation (Chen and Held 2007) during the warm season primarily associated with the role of ozone depletion (O13; Delworth and Zeng 2014; Polvani et al. 2011; among others). Conversely, during the cold season, the subtropical westerly jet is shifted slightly poleward, and the subpolar westerly jet is shifted equatorward, in agreement with Archer and Caldeira (2008). This behavior is strongly associated with the lower-tropospheric warming related to the increasing concentration of GHGs that is in agreement with O13 (not shown).

b. *Changes as depicted by the GFDL CM2.5*

Based on the previous discussion, it is worth exploring to what extent the GFDL CM2.5 simulation is able to reproduce both the observed precipitation changes and underlying mechanisms. The zonal-mean precipitation change, as depicted by the model-weighted ensemble displayed in Fig. 2, suggests a good agreement compared with the observations. The model captures the increase of rainfall over the high latitudes even more closely than any individual reanalysis during both the warm and cold seasons, although the rainfall reduction at midlatitudes is not clear.

Changes in DV24h, VOR, VORSPHUM, and precipitation from the CM2.5-weighted ensemble for the extended SH summer and winter seasons are shown in Figs. 6 and 7, respectively. During the extended summer season (Fig. 6), the CM2.5 ensemble broadly reproduces the pattern of precipitation change depicted by both REwens and GPCP, with rainfall increase at the high latitudes of the SH and a weak rainfall decrease at middle-to-subtropical latitudes. However, the simulated changes are weaker compared with the changes depicted by the REwens. Note also that the model does not reproduce the characteristic zonal symmetry of the precipitation change depicted in the REwens. Changes in DV24h are consistent with changes in precipitation; however, changes in VOR are very subtle almost everywhere. Moreover, changes in VORSPHUM are also consistent with changes in rainfall, suggesting that the moisture increase, probably associated with warmer sea surface temperatures [as discussed in Delworth et al. (2012)], contributes to the precipitation increase at high latitudes. Inspection of changes in the specific humidity (not shown) reveals an overall increase, which may contribute to the changes in VORSPHUM. This behavior disagrees with what was found for the REwens, in that the high-latitude moistening was associated with increased eddy activity due to the poleward shift of the storm track and not with moisture increase.

For the extended winter months (Fig. 7), the model depicts increased rainfall at high latitudes and a weak decline at the subtropics. The most remarkable feature is that rainfall changes are not systematically related with changes in either DV24h or VOR. In particular, the changes in VOR are negative almost everywhere. However, rainfall changes are consistent with changes in VORSPHUM, suggesting that during the winter season the high-latitude rainfall increase is largely associated with the increase of moisture. Consequently, although the model seems to reproduce the precipitation changes, the underlying mechanisms explaining these changes are not the same as for the reanalysis datasets, particularly during the warm season.

4. Summary and conclusions

This study focused on revisiting the features of the recent climate change in the Southern Hemisphere as depicted by a set of reanalyses, with the aim of characterizing a robust precipitation change signal and exploring the underlying physical mechanisms triggering these changes for extended summer and winter seasons. To that end, several metrics quantifying the

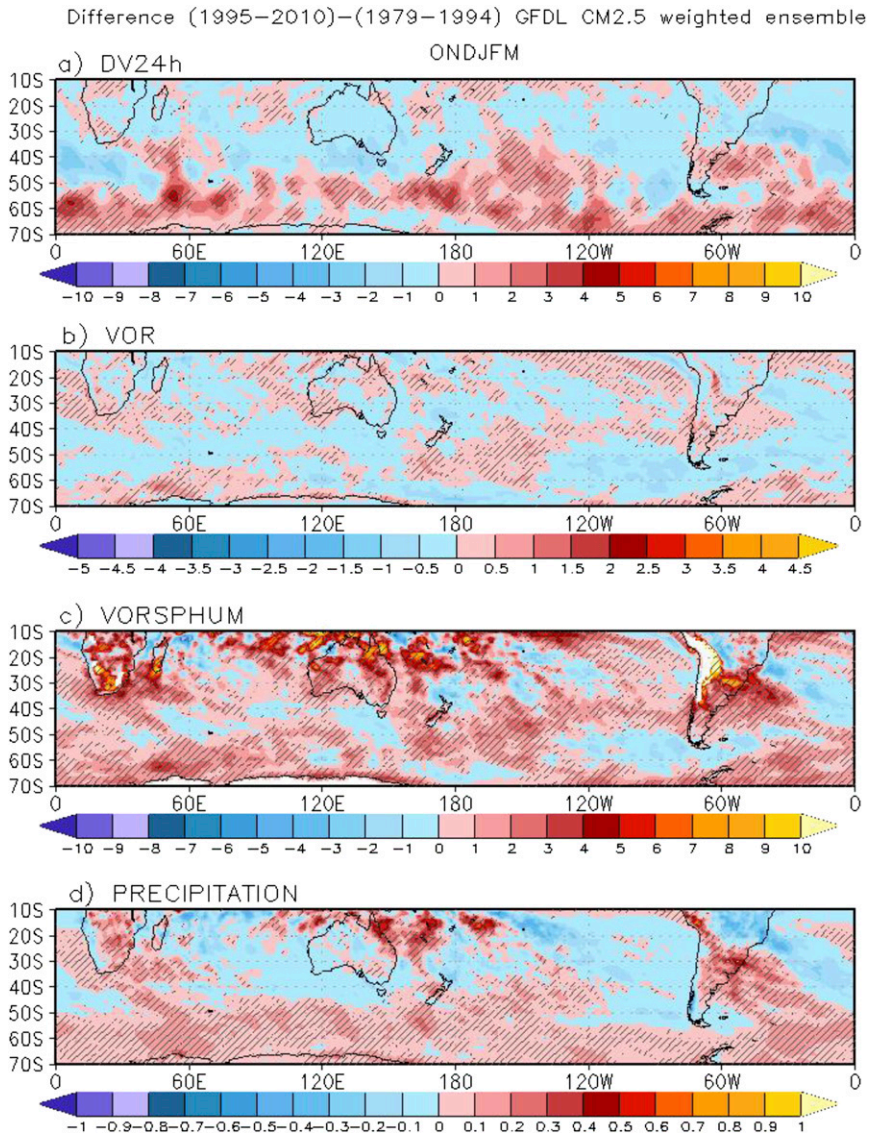

FIG. 6. As in Fig. 3, but for the GFDL CM2.5 ensemble. Hatched areas indicate where 4 out of 5 ensemble members depict positive differences.

eddy activity linked with rainfall were defined. Given the uncertainty in the reanalysis products, particularly for the Southern Hemisphere, a weighted reanalysis ensemble is proposed with the aim of building a robust estimation of the climate change signal based on the most up-to-date reanalyses available. The analysis is mainly focused on middle-to-high latitudes of the Southern Hemisphere, where precipitation is mostly associated with the passage of frontal systems (SO14; Catto et al. 2012). Eddy activity was quantified by different metrics accounting for the cyclonic vorticity, the squared daily tendency of the meridional component of the wind, and the cyclonic vorticity times the specific humidity at 850 hPa. These metrics allowed us to identify whether the change in rainfall could be associated with the change in moisture and/or the change in eddy activity.

A set of five reanalysis datasets for the period 1979–2010 was used: ERA-Interim, MERRA, CFSR, NCEPR2, and 20CR. Even though these datasets are postsatellite era, large differences between individual reanalysis datasets were found when looking at the long-term evolution in several variables. It is well known that the reanalyses are strongly affected by the assimilation system, including the type and quantity of data assimilated. Hence, and in order to account for the uncertainty in the reanalysis products, the reanalyses were combined to build a weighted ensemble in which the weights are

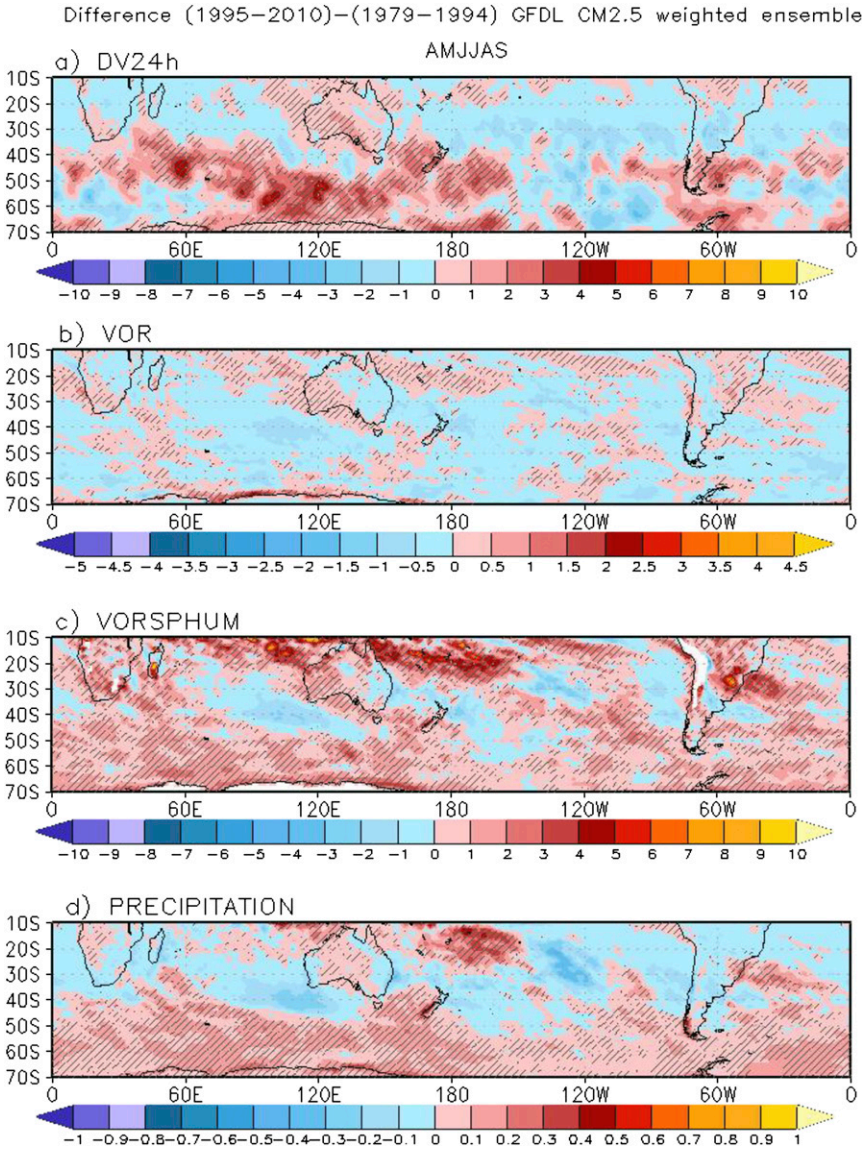

FIG. 7. As in Fig. 6, but for the extended winter season (AMJJAS).

proportional to the inverse of the variance for each individual variable of each dataset. The proposed weighted reanalysis ensemble is expected to give more relevance to those reanalyses with less variance or less uncertainty.

Based on the reanalysis-weighted ensemble, it was found that the climate change signal in the SH for summer months is characterized by the well-known poleward shift of the rainfall belt (increased rainfall over the high latitudes and reduced rainfall over the midlatitudes), in agreement with the observations. The wetting conditions at high latitudes and drying conditions at midlatitudes were found to be quasi-zonally symmetric and related with the changes in the eddy activity, which are in turn associated with the poleward shift of the westerlies. This change may be attributed mostly to ozone depletion during the period analyzed.

For the winter season, wetting and drying conditions at high and middle latitudes, respectively, are also apparent, but there are large zonal asymmetries in the rainfall change pattern. Moreover, changes in eddy activity and moisture at the lower troposphere contribute to rainfall changes. The poleward shift of the subtropical westerlies is weaker than in summer, and the largest control of this change is related to the increase in the concentration of GHGs. The increase of latent heat flux over the southern oceans during the most recent period (Yu et al. 2012) may lead to increased specific humidity, which favors increased rainfall at the high latitudes.

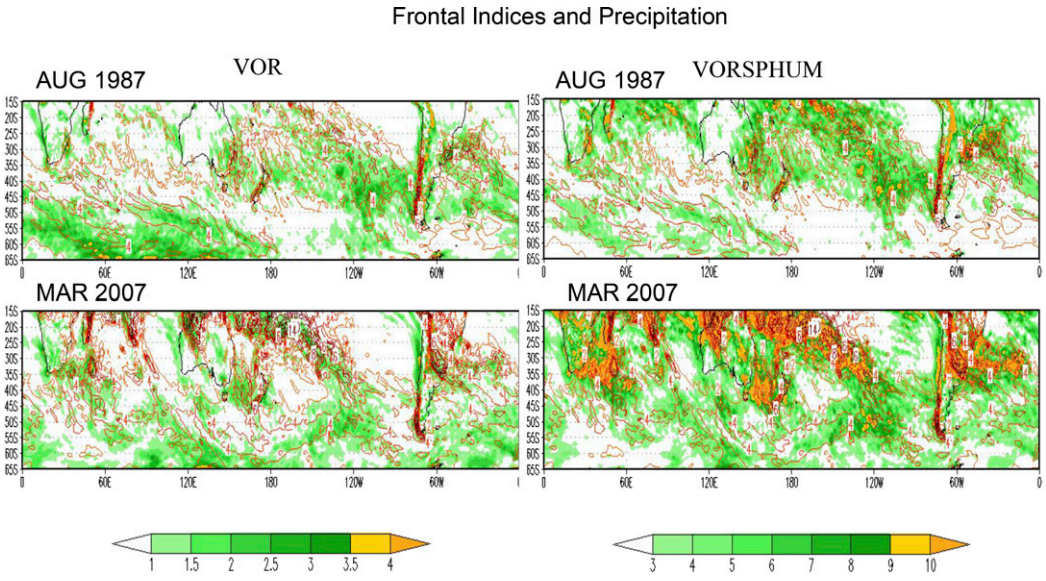

FIG. A1. Examples of the connection between frontal indices and monthly precipitation for (top) August 1987 and (bottom) March 2007 from the CFSR dataset: (left) the VOR index (shaded; $10^5\,s^{-1}$) and (right) the VORSPHUM index (shaded; $10^8\,s^{-1}$). Precipitation is contoured in red (interval 2 mm day^{-1}) and the minimum contour is 2 mm day^{-1}.

Overall, the diagnosis built from the reanalysis-weighted ensemble allowed us to elaborate a dynamically consistent picture of the recent changes in the middle and high latitudes of the SH, in particular, reinforcing the robustness of precipitation changes associated with changes in the eddy activity and moisture availability and also identifying the drivers of the circulation change. The proposed combination of reanalyses to characterize the climate change signal in the SH is valuable in order to set a reference behavior to validate climate model simulations.

Accordingly, we have made this attempt in order to validate the behavior of GFDL CM2.5 in reproducing the climate change signal in the SH and the underlying mechanisms explaining its behavior. It was found that the pattern of precipitation change from the GFDL CM2.5 simulation generally agrees with the changes depicted by the reanalysis-weighted ensemble; however, the increase of moisture at the lower levels is the main driver of the rainfall increase at the high latitudes during both summer and cold seasons. Accordingly, although the model simulates a rainfall change consistent with what the observations show, the underlying mechanisms are not consistent with the picture that emerged using the reanalysis-weighted ensemble.

One last consideration on the methodology used to build the ensemble proposed in this study is that, although it has been shown that it allowed building a robust climate change signal, the choice of the weights, proportional to the inverse of the variance, is certainly not the only option. It has the advantage of reducing the uncertainty in the climatological mean values; however, it is also recognized that a reanalysis with low variance should not be considered per se more reliable than a reanalysis with large variance. The best option should come from comparing the variance of the reanalysis against the variance of the observations; however, because of the lack of global observations, this is not possible. Hence, the choice of the weights proposed is one possible option, but there may be other options as well. For instance, in Mitchell et al. (2015) various reanalysis datasets were intercompared to evaluate the signature of several natural forcings, and an ensemble of reanalyses was built without weights.

Finally, the methodology proposed in this study may also be valuable to produce a weighted ensemble of climate model simulations to evaluate both the capability of the models in simulating observed trends, as has been done in this study using a weighted ensemble for a single model, and the future climate change signal in response to anthropogenic forcings.

Acknowledgments. The authors are grateful to Ronald Stouffer for insightful comments on the manuscript and Fanrong Zeng for providing data from GFDL models. This work has been supported by the grants FONCyT—PICT-2012-1972, CONICET PIP 112-201101-00189, and UBACYT2014 20020130200233BA, Raices Programme from MINCYT, and the National Oceanic and Atmospheric Administration of the U.S. Department of Commerce. The statements, findings, conclusions, and recommendations are

those of the author(s) and do not necessarily reflect the views of the National Oceanic and Atmospheric Administration or the U.S. Department of Commerce. The authors acknowledge downloading the following datasets: NCEP–DOE AMIP-II reanalysis, GPCP, and CMAP data provided by the NOAA/OAR/ESRL Physical Sciences Division, Boulder, Colorado, from their website (http://www.esrl.noaa.gov/psd/data/). The authors also thank the three anonymous reviewers for their very useful comments and suggestions, which greatly contributed to improve the manuscript.

APPENDIX A

On the Connection between Dynamic and Thermodynamic Metrics and Rainfall

It has been stated in previous sections that several metrics accounting for the eddy activity together with the moisture availability (referred to as VOR and VORSPHUM) were used because they are dynamically and thermodynamically associated with precipitation at the extratropical latitudes of the SH. Moreover, it has already been shown (SO14; Catto et al. 2012) that much of the 90% of the annual precipitation over the storm tracks in the SH is associated with frontal systems. Frontal systems at extratropical latitudes are usually associated with a cyclonic vorticity center, and hence the VOR metric represents the dynamical triggering mechanisms of rainfall events. However, the moisture availability at the lower levels of the troposphere may also impact rainfall so that VORSPHUM, calculated as the monthly mean cyclonic vorticity times the monthly mean specific humidity at 850 hPa, represents the thermodynamical mechanism related to precipitation events.

In Fig. A1 the connection between rainfall and the metrics referred to above are shown for two individual months corresponding to August 1987 and March 2007, respectively. For the two selected periods, the close connection between monthly rainfall and VORSPHUM at the extratropical latitudes of the SH is apparent even for two months belonging to either cold or warm seasons. Figure A1 also suggests that larger rainfall amounts occur over areas where VOR and VORSPHUM are larger, particularly between 50° and 25°S.

APPENDIX B

On the Weights of the REwens

The normalized weights to build the REwens, computed as the percent contribution of each reanalysis to the weighted ensemble for each variable, are shown in Fig. B1.

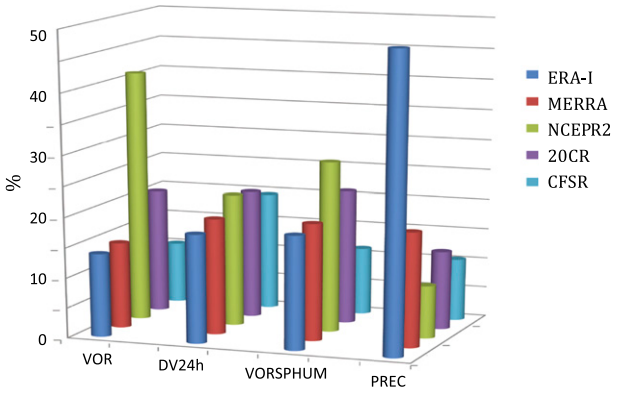

FIG. B1. Percentage of an individual reanalysis' contribution to the ensemble for each metric.

In the ideal case in which all reanalyses have the same variance for a given variable, the weights for all reanalyses should be similar, and the contribution of each reanalysis (out of five) to the variance of the ensemble should be close to 20%. If this happens, then one could suggest that the uncertainty is low and the weighted ensemble is close to the unweighted ensemble, as used in Mitchell et al. (2015).

Note that, for those variables representing the synoptic-scale processes, such as DV24h, a variable expected to be well resolved by any reanalysis regardless of the horizontal resolution, the contribution of each reanalysis to the total variance is close to 20%. However, precipitation or VOR, which are more resolution-dependent variables, are expected to have less variance for those reanalyses with lower resolution and, consequently, higher weights.

As can be seen in Fig. B1, in general, the weights for each variable for all reanalyses are similar, except for precipitation and VOR. The large weight of ERA-I for precipitation is because it has much lower variance compared with the other datasets. For VOR, NCEPR2 has the lowest resolution, it accounts for the lowest variance and, hence, the largest weight. For DV24h, the weights between the set of reanalyses are close to each other, and each reanalysis contributes (approximately) 20% to the ensemble variance. For comparison purposes, the weights for all the metrics have also been computed for the Northern Hemisphere, and it was found that every reanalysis contributes similarly to the variance of the ensemble for all the variables evaluated here (not shown).

The REwens is expected to represent better the mean value and even a climate signal of any variable compared with a simple ensemble because it prevents possible spurious variability that may arise because of changes in the amount or type of data assimilated in an individual reanalysis, giving less weight to those reanalyses with higher variability.

REFERENCES

Arblaster, J., and G. Meehl, 2006: Contributions of external forcings to southern annular mode trends. *J. Climate*, **19**, 2896–2905, doi:10.1175/JCLI3774.1.

——, ——, and D. Karoly, 2011: Future climate change in the Southern Hemisphere: Competing effects of ozone and greenhouse gases. *Geophys. Res. Lett.*, **38**, L02701, doi:10.1029/2010GL045384.

Archer, C. L., and K. Caldeira, 2008: Historical trends in the jet streams. *Geophys. Res. Lett.*, **35**, L08803, doi:10.1029/2008GL033614.

Bender, F. A. M., V. Ramanathan, and G. Tselioudis, 2012: Changes in extratropical storm track cloudiness 1983–2008: Observational support for a poleward shift. *Climate Dyn.*, **38**, 2037–2053, doi:10.1007/s00382-011-1065-6.

Bengtsson, L., and K. I. Hodges, 2011: On the evaluation of temperature trends in the tropical troposphere. *Climate Dyn.*, **36**, 419–439, doi:10.1007/s00382-009-0680-y.

Bosilovich, M. G., J. Chen, F. R. Robertson, and R. F. Adler, 2008: Evaluation of global precipitation in reanalyses. *J. Appl. Meteor. Climatol*, **47**, 2279–2299, doi:10.1175/2008JAMC1921.1.

Cai, W., T. Cowan, and M. Thatcher, 2012: Rainfall reductions over Southern Hemisphere semi-arid regions: The role of subtropical dry zone expansion. *Sci. Rep.*, **2**, 702, doi:10.1038/srep00702.

Catto, J. L., C. Jakob, G. Berry, and N. Nicholls, 2012: Relating global precipitation to atmospheric fronts. *Geophys. Res. Lett.*, **39**, L10805, doi:10.1029/2012GL051736.

Chang, E. K. M., Y. Guo, X. Xia, and M. Zheng, 2013: Storm-track activity in IPCC AR4/CMIP3 model simulations. *J. Climate*, **26**, 246–260, doi:10.1175/JCLI-D-11-00707.1.

Chelliah, M., W. Ebisuzaki, S. Weaver, and A. Kumar, 2011: Evaluating the tropospheric variability in National Centers for Environmental Prediction's climate forecast system reanalysis. *J. Geophys. Res.*, **116**, D17017, doi:10.1029/2011JD015707.

Chen, G., and I. M. Held, 2007: Phase speed spectra and the recent poleward shift of Southern Hemisphere surface westerlies. *Geophys. Res. Lett.*, **34**, L21805, doi:10.1029/2007GL031200.

Compo, G. P., and Coauthors, 2011: The Twentieth Century Reanalysis Project. *Quart. J. Roy. Meteor. Soc.*, **137**, 1–28, doi:10.1002/qj.776.

Dee, D. P., and Coauthors, 2011: The ERA-Interim Reanalysis: Configuration and performance of the data assimilation system. *Quart. J. Roy. Meteor. Soc.*, **137**, 553–597, doi:10.1002/qj.828.

Delworth, T. L., and F. Zeng, 2014: Regional rainfall decline in Australia attributed to anthropogenic greenhouse gases and ozone levels. *Nat. Geosci.*, **7**, 583–587, doi:10.1038/ngeo2201.

——, and Coauthors, 2012: Simulated climate and climate change in the GFDL CM2.5 high-resolution coupled climate model. *J. Climate*, **25**, 2755–2781, doi:10.1175/JCLI-D-11-00316.1.

Fu, Q., C. M. Johanson, J. M. Wallace, and T. Reitchler, 2006: Enhanced mid-latitude tropospheric warming in satellite measurements. *Science*, **312**, 1179, doi:10.1126/science.1125566.

Fyfe, J. C., N. P. Gillett, and G. J. Marshall, 2012: Human influence on extratropical Southern Hemisphere summer precipitation. *Geophys. Res. Lett.*, **39**, L23711, doi:10.1029/2012GL054199.

Gastineau, G., L. Li, and H. Le Treut, 2009: The Hadley and Walker circulation changes in global warming conditions described by idealized atmospheric simulations. *J. Climate*, **22**, 3993–4013, doi:10.1175/2009JCLI2794.1.

Gillett, N. P., J. C. Fyfe, and D. E. Parker, 2013: Attribution of observed sea level pressure trends to greenhouse gas, aerosol, and ozone changes. *Geophys. Res. Lett.*, **40**, 2302–2306, doi:10.1002/grl.50500.

Huffman, G. J., R. F. Adler, D. T. Bolvin, and G. Gu, 2009: Improving the global precipitation record: GPCP Version 2.1. *Geophys. Res. Lett.*, **36**, L17808, doi:10.1029/2009GL040000.

Kanamitsu, M., W. Ebisuzaki, J. Woollen, S.-K. Yang, J. J. Hnilo, M. Fiorino, and G. L. Potter, 2002: NCEP–DOE AMIP-II reanalysis (R-2). *Bull. Amer. Meteor. Soc.*, **83**, 1631–1643, doi:10.1175/BAMS-83-11-1631.

Lorenz, C., and H. Kunstmann, 2012: The hydrological cycle in three state-of-the-art reanalyses: Intercomparison and performance analysis. *J. Hydrometeor.*, **13**, 1397–1420, doi:10.1175/JHM-D-11-088.1.

Mitchell, D. M., and Coauthors, 2015: Signatures of naturally induced variability in the atmosphere using multiple reanalysis datasets. *Quart. J. Roy. Meteor. Soc.*, **141**, 2011–2031, doi:10.1002/qj.2492.

Orlanski, I., 2013: What controls recent changes in the circulation of the Southern Hemisphere: Polar stratospheric or equatorial surface temperatures? *Atmos. Climate Sci.*, **3**, 497–509, doi:10.4236/acs.2013.34052.

Paek, H., and H.-P. Huang, 2012: A comparison of the interannual variability in atmospheric angular momentum and length-of-day using multiple reanalysis data sets. *J. Geophys. Res.*, **117**, D20102, doi:10.1029/2012JD018105.

Polvani, L. M., D. W. Waugh, G. J. P. Correa, and S. W. Son, 2011: Stratospheric ozone depletion: The main driver of twentieth-century atmospheric circulation changes in the Southern Hemisphere. *J. Climate*, **24**, 795–812, doi:10.1175/2010JCLI3772.1.

Rienecker, M. M., and Coauthors, 2011: MERRA: NASA's Modern-Era Retrospective Analysis for Research and Applications. *J. Climate*, **24**, 3624–3648, doi:10.1175/JCLI-D-11-00015.1.

Saha, S., and Coauthors, 2010: The NCEP Climate Forecast System Reanalysis. *Bull. Amer. Meteor. Soc.*, **91**, 1015–1057, doi:10.1175/2010BAMS3001.1.

Solman, S. A., and I. Orlanski, 2014: Poleward shift and change of frontal activity in the Southern Hemisphere over the last 40 years. *J. Atmos. Sci.*, **71**, 539–552, doi:10.1175/JAS-D-13-0105.1.

Thompson, D. W. J., and S. Solomon, 2002: Interpretation of recent Southern Hemisphere climate change. *Science*, **296**, 895–899, doi:10.1126/science.1069270.

Trenberth, K. E., and J. T. Fasullo, 2013: An apparent hiatus in global warming? *Earth's Future*, **1**, 19–32, doi:10.1002/2013EF000165.

——, L. Smith, T. Qian, A. Dai, and J. Fasullo, 2007: Estimates of the global water budget and its annual cycle using observational and model data. *J. Hydrometeor.*, **8**, 758–769, doi:10.1175/JHM600.1.

——, J. T. Fasullo, and J. Mackaro, 2011: Atmospheric moisture trans- ports from ocean to land and global energy flows in reanalyses. *J. Climate*, **24**, 4907–4924, doi:10.1175/2011JCLI4171.1.

Xie, P., and P. A. Arkin, 1997: Global precipitation: A 17-year monthly analysis based on gauge observations, satellite estimates, and numerical model outputs. *Bull. Amer. Meteor. Soc.*, **78**, 2539–2558, doi:10.1175/1520-0477(1997)078<2539:GPAYMA>2.0.CO;2.

Yu, L., and Coauthors, 2012: Trends in latent and sensible heat fluxes over the Southern Ocean. *Atmos. Climate Sci.*, **2**, 159–173, doi:10.4236/acs.2012.22017.